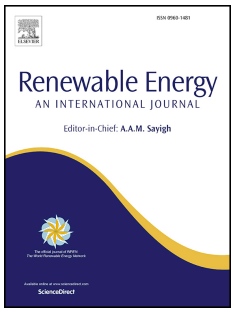
CORA Cork Open Research Archive
Cartlann Taighde Oscailte Chorcaí

Title	Development of a free heaving OWC model with non-linear PTO interaction
Authors	O'Connell, Ken;Thiebaut, Florent;Kelly, Ger;Cashman, Andrew
Publication date	2017-10-12
Original Citation	O'Connell, K., Thiebaut, F., Kelly, G. and Cashman, A. (2018) 'Development of a free heaving OWC model with non-linear PTO interaction', Renewable Energy, 117, pp.108-115. doi:10.1016/j.renene.2017.10.027
Type of publication	Article (peer-reviewed)
Link to publisher's version	10.1016/j.renene.2017.10.027
Rights	© 2017, Elsevier Ltd. All rights reserved.This manuscript version is made available under the CC-BY-NC-ND 4.0 license. - https://creativecommons.org/licenses/by-nc-nd/4.0/
Download date	2026-11-06 03:39:44
Item downloaded from	https://hdl.handle.net/10468/5833



UCC
University College Cork, Ireland
Coláiste na hOllscoile Corcaigh

Accepted Manuscript



Development of a free heaving OWC model with non-linear PTO interaction

Ken O. Connell, Andrew Cashman, Florent Thiebaut, Ger Kelly

PII: S0960-1481(17)30989-8

DOI: 10.1016/j.renene.2017.10.027

Reference: RENE 9315

To appear in: *Renewable Energy*

Received Date: 4 August 2016

Revised Date: 2 October 2017

Accepted Date: 9 October 2017

Please cite this article as: Connell KO, Cashman A, Thiebaut F, Kelly G, Development of a free heaving OWC model with non-linear PTO interaction, *Renewable Energy* (2017), doi: 10.1016/j.renene.2017.10.027.

This is a PDF file of an unedited manuscript that has been accepted for publication. As a service to our customers we are providing this early version of the manuscript. The manuscript will undergo copyediting, typesetting, and review of the resulting proof before it is published in its final form. Please note that during the production process errors may be discovered which could affect the content, and all legal disclaimers that apply to the journal pertain.

ACCEPTED MANUSCRIPT

Development of a free heaving OWC model with non-linear PTO interaction

Ken O Connell[a], Andrew Cashman[a,*], Florent Thiebaut[b], Ger Kelly[a]

[a] *Mechanical, Biomedical & Manufacturing Engineering Department, Cork Institute of Technology (CIT), Cork, Ireland.*
[b] *MaREI Centre, Environmental Research Institute, University College Cork (UCC), Ringaskiddy, Co Cork, Ireland.*

Abstract

This paper presents the development of a Computational Fluid Dynamics (CFD) model for a free heaving Oscillating Water Column (OWC) spar buoy with non-linear Power Take Off (PTO). Firstly, a freely heaving barge was applied to a 2D Numerical Wave Tank (NWT), used to validate a 1 Degree Of Freedom (DOF) modelling methodology. Multiple sets of regular waves were used to assess the heave response compared to previous experimental and numerical studies. In parallel, the NWT was extended to 3D where analyses of incident waves have been conducted to ensure accurate waves are portrayed. A PTO boundary condition was created to replicate a non-linear impulse turbine, typically simulated by an orifice plate in scaled models. The PTO boundary was compared and validated using experimental data. Finally, a comprehensive system comprising of the 3D NWT, 1DOF set-up and non-linear PTO allowed the development of a heave-only OWC spar buoy model with a non-linear PTO. Experiments completed by UCC MaREI centre in LIR-NOTF ocean wave basin under FP7 MARINET project is detailed and used to validate the comprehensive model. A range of regular waves were applied and responses of heave and chamber pressures were compared to experimental data, which showed excellent correlation.

Keywords: Computational Fluid Dynamics (CFD), Numerical Wave Tank (NWT), Wave Energy Converter (WEC), Freely heaving Oscillating Water Column (OWC)

1. Introduction

Wave Energy Converter (WEC) devices are used to convert the oceans wave energy into usable electrical energy. The Oscillating Water Column (OWC) is said to be one of the most researched devices from the WEC field [1]. The structure contains an opening which is submerged beneath the ocean's surface allowing incident waves to enter the chamber. Waves then periodically force a column of air through a self-rectifying turbine located on the upper end of the chamber. This turbine is combined with an electrical generator to form a Power Take Off device (PTO). These WEC devices can be located on shorelines, designed into breakwaters or as offshore floating devices. The use of shoreline OWCs allows ease of connection and construction, but has limited optimal sites due to the energy dissipation from shoaling waves [2].

Offshore OWC spar buoy devices have a unique characteristic of two fundamental frequencies of both the chamber and structural response. Tuning these frequencies allows for the performance range of the device to be optimised over a larger bandwidth of sea states, or amplified for a smaller bandwidth. The spar buoy is considered to be a very elegant design where, due to its simplicity and axis-symmetry, it is insensitive to wave direction. The device is also considered as low risk and the most economic of the floating OWC devices [1, 3]. Offshore OWCs are very advantageous due to their ability to harness energy in deep water and to utilise the space for large arrays of systems.

*Corresponding Author
Email addresses: ken.c.oconnell@gmail.com (Ken O Connell), andrew.cashman@cit.ie (Andrew Cashman), ger.kelly@cit.ie (Ger Kelly)

ACCEPTED MANUSCRIPT

Many prototypes of the shoreline OWC devices have been designed and tested at full scale to show their ability as future WECs. A 400kW shoreline European pilot plant was constructed on the island of Pico in the Azores [4]. Another shoreline OWC was established on Islay, Scotland, which used a 500kW Wells turbine [5]. Many offshore OWC devices have been constructed and tested throughout the world. A 1:4 scale backward bent duct buoy was tested first with a Wells turbine and then an impulse turbine in Galway, Ireland [5]. An Australian company Oceanlinx tested a 1:3 scale floating OWC, known as Mk3, in 2010 [5].

Much literature exists outlining the methods used by designers to optimise the performance of these devices such as frequency and state-space models or more complex time domain models. Computational Fluid Dynamics (CFD) uses the Navier-Stokes equations to solve fluid motion in the time domain. This method allows for non-linear interactions simulated due to real fluid effects, such as vortices, viscous effects, turbulence effects, etc [5, 6]. The inclusion of these flow phenomenon will allow a higher accuracy to be attained when analysing Fluid-Structure Interactions (FSI) and device performance.

CFD has been extensively used to analyse and optimise the performance of shoreline and offshore OWC devices. Bouali and Larbi analyse the impact of the draught geometry on the performance of a shoreline OWC [7]. Linear PTO influence on the performance of a shoreline OWC is assessed by Kamath et al. [8]. Dider et al. analyses the damping impact on the performance of a static 3D offshore OWC [9]. Dider et al. show the importance of matching the correct PTO damping to obtain higher efficiencies. Luo et al. employs a 1 Degree Of Freedom (DOF) model to analyse linear mooring and PTO constraints on the performance of an offshore OWC in 2D [10]. Luo et al. shows both PTO and mooring selection plays a large influence on the optimum device performance.

The paper presented here focuses on the development of a 3D CFD model to accurately represent the dynamic response of a free floating spar buoy with a non-linear PTO. To the authors knowledge, this is the first comprehensive dynamic CFD model of an OWC spar buoy. The model is developed in stages beginning with the Numerical Wave Tank (NWT) to allow accurate propagation of incident waves. A dynamic mesh is used to permit the 1DOF free heaving, of a simulated barge in the 2D NWT. Validation of the 1DOF modelling methodology against results of others proves the accuracy prior to inclusion of an OWC spar buoy. In parallel, a 3D NWT is assessed against linear wave theory which is required to include the geometrical requirements of the axis-symmetric spar buoy. A non-linear PTO is developed and validated using real orifice data and further implemented into the spar buoy model. Coupling all previous stages allows for an in-depth numerical model to be realised. Experimental validation was completed to assess the accuracy of the numerical model and data is provided by the MaREI Centre in LIR-NOTF under the FP7 MARINET Project. Regular monochromatic waves are applied to determine the coupled dynamic response of the OWC device. Heave and pressure characteristics of the CFD model are discussed and compared to experimental results assessing the accuracy of the model to a real situation.

2. Numerical model development

2.1. 2D NWT set-up

A NWT is created using a commercial CFD package, ANSYS Fluent 16.0, which solves the Navier-Stokes equations. The Volume Of Fluid (VOF) method is used to resolve the multiphase fluid flow within the computational domain. A transient model is created using a two-phase 2D domain. An open channel wave boundary condition is applied upstream to allow the propagation of incident waves, whilst the numerical beach scheme is applied downstream to dissipate the waves before they leave the domain. This prevents reflection from occurring at the downstream boundary. An open channel is applied to permit the dissipated waves to exit the domain, retaining a constant mean free surface. Atmospheric conditions are applied using a pressure-outlet boundary and no-slip conditions are used for the bed of the NWT.

A structured quadrilateral mesh type is used to discretize the NWT using ANSYS's meshing tool. The mesh is specified using dimensionless criteria of 20 cells per wave height and 50 cells per wavelength as recommended by O Connell and Cashman [11] following a discretization error analysis. Velocities and free surface elevation error were evaluated to be below 1% in the study. Time steps were allowed to vary using the dimensionless Courant-Friedrichs-Lewy (CFL) number. Therefore, the time step size is dependent on fluid

velocity, cell size and a constant CFL number. Typically the CFL number is kept below 2 for 2D simulations and below 1 for 3D simulations [12]. A low CFL number of 0.1 is used throughout the study presented in this paper which allows for time dependent flow phenomena to be modelled with a high resolution and thus ensuring a solution independent of time step size was obtained. Likewise, residuals are required to drop 4 orders of magnitude before convergence criteria is satisfied to ensure highly accurate results.

2.2. 1DOF modelling methodology

A free floating barge is applied to the previously specified 2D NWT in order to create an accurate freely heaving 1DOF model. The model set-up is based on analytical and experimental work completed by Nojiri and Murayama [13]. Koo and Kim [14] and Luo et. al. [15] adopted this approach to validate their numerical models along with Tanizawa and Minami [16]. The numerical domain is set-up as shown in Figure 1, where the floating structure is only constrained to heave freely. The model consists of a tank 8λ long with a depth of λ, where λ is the incident wavelength. Wave generation occurs on the left of the tank and subsequently damped using a numerical beach scheme on the opposite end. This model allows the validation of the FSI for free floating structures using the 1DOF numerical model. Accurate representation of an FSI is critical to subsequent work which derives its absorbed power from both the heaving structure and incident wave interaction.

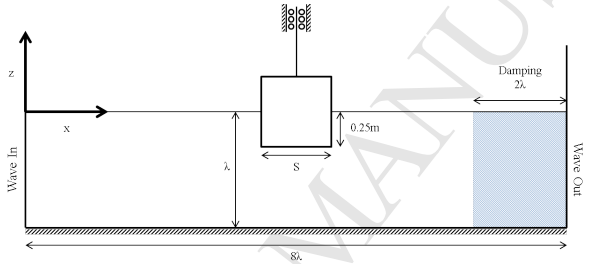


Figure 1: Heave only barge schematic set-up.

A dynamic mesh is applied to the domain to allow the barge to oscillate in heave mode. The smoothing scheme method is used to remesh the domain at each iteration to fully resolve the hydrodynamic motion. The use of a remeshing scheme significantly increases the computational requirements and in turn the solving time. Turbulence modelling used here employed a realizable $\kappa - \epsilon$ model to reproduce turbulence effects of the fluid flow. Monochromatic linear waves were applied to the domain to assess the FSI of the barge with a width of $S = 0.5$m and mass of 125kg. Regular waves with height H=0.02m and periods of between 0.4-2s are allowed to propagate through the domain. Simulations are deemed complete when the heave amplitude of the barge reaches a quasi-steady state and remained consistent. The heave Response Amplitude Operator (RAO) is the ratio of heave amplitude of the barge over the incident wave amplitude. The results of the heave RAO are reproduced in comparison with the results of other studies in Figure 2 with respect to the applied incident wave period.

Using the described modelling approach, good correlation of the RAO is seen between the present CFD model and results of the other studies shown in Figure 2, hence validating the modelling approach employed here. Thus, the 1DOF modelling methodology outlined in this section accurately portrays the FSI of a freely floating body with incident waves. The modelling approach is further applied to FSI analyses of a floating, heave only, spar buoy structure in Section 2.5.

2.3. 3D NWT set-up

The axis-symmetric geometry of a spar buoy OWC can not be represented accurately in 2 dimensions. Therefore, this justifies the move into utilising a 3D computational domain for an accurate FSI to occur. Furthermore, reducing reflections from the device of interest in 2D is necessary for accurate incident waves. Diffraction within the 3D domain can permit transmission of waves past the device with negligible reflections. Thus, using a 3D domain allows for an accurate portrayal of the response from the spar buoy geometry.

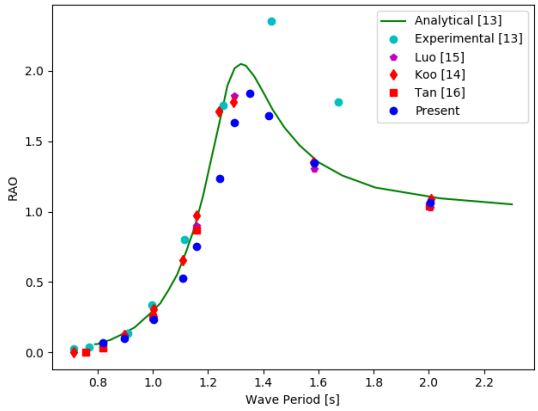


Figure 2: Comparison of RAO results for free heaving barge.

Progression of the 2D NWT into 3D requires the analysis of discretization error to ensure accurate propagation of waves. A CFD model is created using the same set-up as in Section 2.1 with a depth of 1m. Multiple regular waves are applied to the domain to assess the free surface elevation and the velocity components beneath the waves. Fluid velocity profiles in both horizontal and vertical directions are plotted at various stages of the propagating wave. Velocity profiles beneath the wave crest, inflection and trough are observed and displayed in Figures 3-5, respectively. These are compared and analysed against linear wave theory.

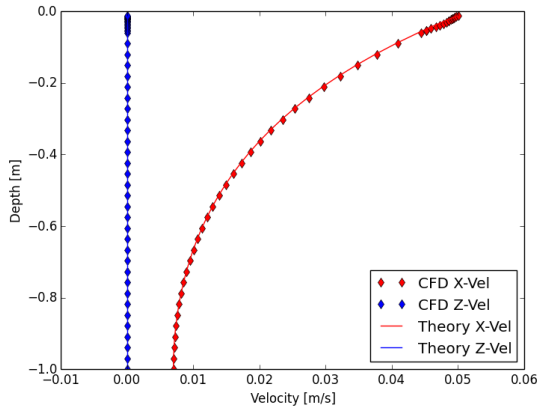


Figure 3: Velocity profiles beneath the wave crest.

Results of the simulations show a high level of accuracy, as the free surface error remains below 0.5% for all simulations. The non-zero velocity profile components, when compared to theory, all showed low error results. The maximum absolute error which occurred across all analyses was a 3.2% deviation from theory, which is considered an acceptable error for incident waves in this study. This high level of accuracy can be seen with excellent correlation to theoretical profiles in Figures 3-5. Simulation times increased significantly with the extension into the third dimension due to the large increase in mesh size.

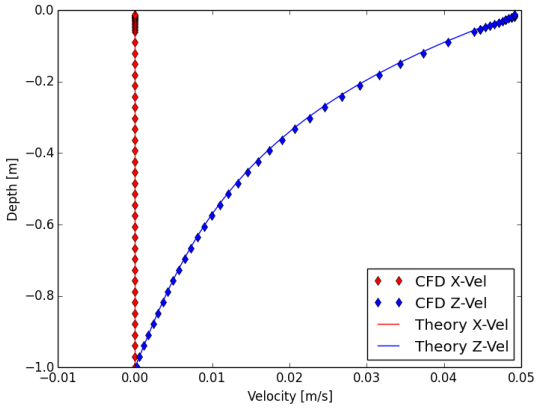


Figure 4: Velocity profiles beneath the waves inflection point.

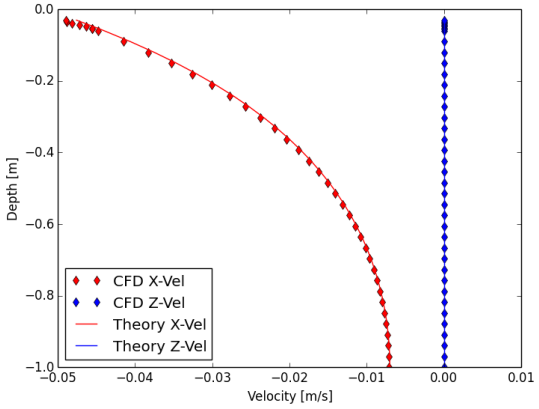


Figure 5: Velocity profiles beneath the trough of the wave.

2.4. PTO development & validation

An impulse turbine is considered to have a non-linear damping influence on the pressure drop, Δp, across the turbine. This can be approximated using equation (1), where the turbine damping coefficient, C_{PTO}, can be considered essentially independent of turbine speed and $\dot{m}$ is the mass flow rate through the turbine. Falcao and Henriques [5] state the rotational speed can be used to tune the resulting turbine efficiency without impacting hydrodynamics.

$$\Delta p \approxeq C_{PTO}\dot{m}^2 \tag{1}$$

Typically an orifice plate is used to simulate a non-linear PTO when conducting experiments at a small scale (usually smaller than 1:4), whereas larger scales can utilise a real turbine [5]. A simple orifice plate can be designed using equation (2) to simulate the impulse turbine at smaller scales.

$$\dot{Q} = C_d a \sqrt{\frac{2\Delta p}{\rho_{air}}} \tag{2}$$

where, a is the area of the orifice opening, C_d is the discharge coefficient, $\dot{Q}$ is the volumetric flow rate and ρ_{air} is the density of air. Using physical orifice plates within CFD simulations creates issues with turbulence modelling and mesh quality. Thus, a PTO boundary condition is created numerically to replace

the use of a physical orifice plate in the simulations, thereby reducing mesh complexity and computational requirements. This allows the replication of back-pressure normally produced by a turbine by a more robust method in CFD. The new boundary condition is assessed against experimental orifice plate data to validate the applicability of using the numerical boundary condition. Experimental equipment and procedure for testing the orifice plate is given in [17] and orifice characteristics are outlined in Table 1. Two test cases with varying piston speeds were conducted here to aid in the validation of the PTO boundary condition.

Table 1: Orifice plate characteristics.

	Case 1	Case 2
Chamber diameter	0.3m	0.3m
Orifice area	0.0106m	0.0106m
Discharge coefficient	0.74	0.74
Stroke	0.05m	0.05m
Period	5s	2.7s

A CFD model comprising of a cylindrical domain with a sinusoidal boundary motion is created. The piston like motion is defined to reciprocate at the same angular velocity and stroke as in the experiment. Two cases are conducted to obtain the orifice pressure drop and further assess the accuracy of the developed boundary condition. A no-slip condition is used for the walls of the chamber with pressure drop within the chamber monitored and plotted in Figures 6 and 7 along with the corresponding experimental data. The model was allowed to run for multiple periods to ensure quasi-steady state is achieved.

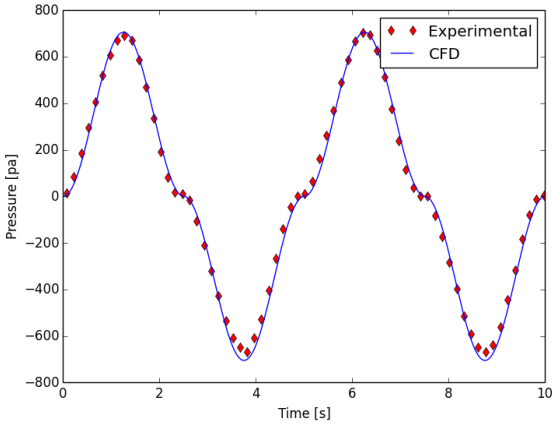


Figure 6: CFD pressure fluctuation compared to experimental data for case 1 at a period of 5s.

Comparison between the simulated orifice and experimental data for both cases show excellent agreement for both case 1 and case 2, seen in Figures 6 and 7. Experimental and numerical results from case 1 are analysed against the theoretical maximum pressure which shows an error of less than 1% for both data sets. Comparative results for case 2 demonstrates a larger deviation of maximum pressure when compared to theory. Up to 8% of an error is observed when comparing the experimental data to theory, whereas CFD simulated results remains to be below 1% when compared to theory. The deviation of peak pressures between numerical and experimental results could be attributed to the incompressible scheme used in the numerical model. This study shows an excellent and accurate response from the PTO boundary condition developed here. Use of this boundary condition is only applicable to small scale incompressible flow problems. The ability to reproduce the response of an orifice plate within a simulation without significant modelling issues while reducing computational demand is a great benefit to future studies and will be applied to the comprehensive OWC model.

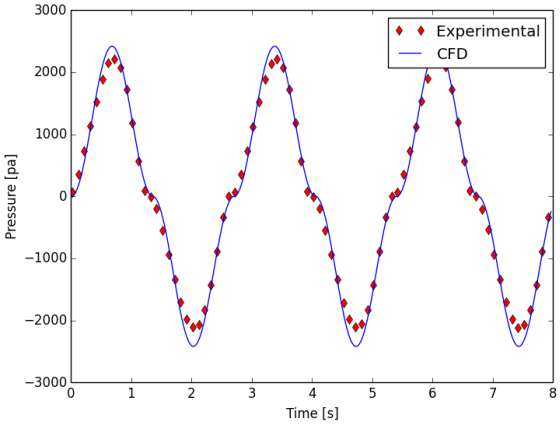


Figure 7: CFD pressure fluctuation compared to experimental data for case 2 at a period of 2.7s.

2.5. OWC model set-up

Coupling the 1DOF modelling methodology with the 3D NWT and the non-linear PTO boundary condition allows a comprehensive FSI model to be realised. Geometry for an axis-symmetric spar buoy, based on the experimental one used in Section 3, is imported into the computational domain. Symmetry is utilised to reduce mesh size in half, reducing computational cost of the simulation. Figure 8 shows the symmetric geometry of the OWC model. The NWT used is 4 wavelengths long, inclusive of 2 wavelengths for the numerical beach scheme. The model is placed 1 wavelength away from the wavemaker boundary and allowed to freely heave using the prescribed 1DOF set-up in Section 2.2. Width and height of the domain are selected to be large enough to not interfere with the response of the floating structure.

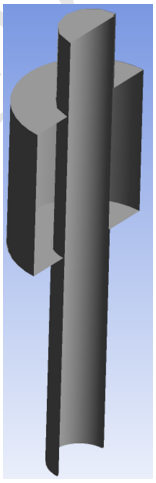


Figure 8: Symmetric model of the OWC spar buoy.

The model uses a CFL number of 0.1 to allow progression of the local time step and to capture the fluid flow at a high resolution. Velocity and displacement magnitudes at monitor points throughout the domain were also examined for convergence, as well as chamber pressure. The PTO damping coefficient is obtained using equation (2) from the orifice used in Section 2.4, which is also used in the experimental work in Section 3.

ACCEPTED MANUSCRIPT

3. Experimental procedure

Experimental testing of a spar type OWC was carried out in January 2015 by the MaREI centre in the LIR-NOTF Ocean basin at $1:50^{th}$ scale. The trials were initially performed under the Round Robin testing, as part of the FP7 Marinet project, where five facilities operating ocean wave basins carried out trials using the same input characteristics in order to compare the resulting motion and power characteristics. This section presents the experimental set-up and wave characteristics used in the trials.

3.1. Wave basin dimensions and test location

The wave basin in LIR-NOTFwas built specifically to help the development of wave energy devices and designed to test wave energy devices around 1:40th to 1:100th scale. It is equipped with 40 independent paddles hinged at 0.7m water depth and is capable of recreating regular waves or real ocean sea states in one direction or using directional spreading functions. The paddles are Edinburgh Design built and equipped with active absorption system. A schematic of a half section of the ocean basin is shown in Figure 9.

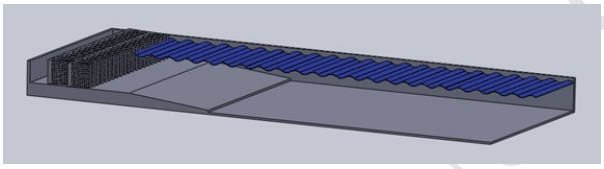


Figure 9: Overview of a half section of the basin.

3.2. Experimental model characteristics

The experimental model used in the trial is a vertical spar type OWC with a 10mm orifice for air power dissipation representing a non-linear type PTO system such as an impulse turbine. The main dimensions are illustrated in Figure 10 and all the measured characteristics are listed in Table 2. This table includes the values at tank scale and their equivalent at full scale using the Froude scaling method. The experimental model is tested at $1{:}50^{th}$ scale and used to validate the numerical model in this paper.

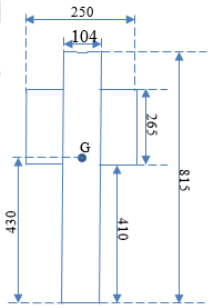


Figure 10: OWC model drawing and dimensions (in mm).

3.3. Experimental set-up in the wave basin

The OWC model is placed at the centre of the basin, 6.75m from the paddle array, in the 1m depth section. It is free floating and moored at the water level with three mooring lines, 120 degrees angle spreading on the horizontal plane. Each mooring line is composed of a horizontal light rope 1.45m length connecting the OWC to an additional mooring float. The float is then connected to the basin floor through a catenary type line using a 3m galvanised steel chain. This set-up was designed to reduce the impact of the mooring system on the heave and pitch motions and restrict large surge, sway and yaw motions. A picture of the final setup is shown in Figure 11.

Table 2: Characteristics of the experimental OWC model.

	Measured 50th scale	
Parameter	Full scale	50th scale
Chamber height	41.25 m	825 mm
Float height	13.25 m	265 mm
Height of the float bottom	20.5m	410 mm
Chamber internal diameter	5.2m	104 mm
Chamber wall thickness	0.15m	3 mm
Float diameter	12.5 m	250 mm
Orifice diameter	530	10.6 mm
Orifice Coefficient Cd	0.74	0.74
Height of the centre of gravity	21.5	430 mm
Total mass	811.25 Tonnes	6.49 kg
Mass of the OWC chamber	180.75 Tonnes	1.446 kg
Mass of the float	29.5 Tonnes	0.236 kg
Mass of the added lead weights	601 Tonnes	4.808 kg
Moment of inertia, XX and YY	198 906 Tonnes.m^2	0.6365 kg.m^2
Heave period	7	1 s
Pitch period	23.7	3.35 s

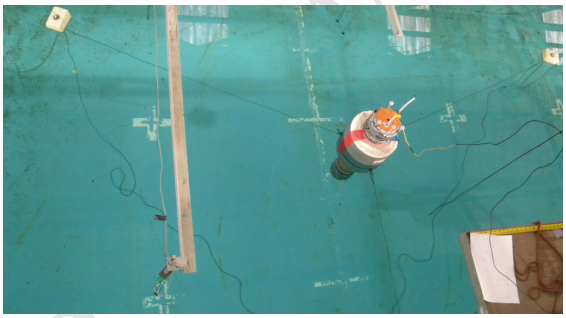


Figure 11: Experimental set-up in the ocean basin.

3.4. Sensors and acquisition system

A data acquisition system and a series of sensors were used during the trials. The measured parameters relevant for this study include the air pressure within the OWC chamber and the 6DOF motion of the spar buoy. All data time series were recorded at a rate of 32Hz with a CompactRio system from National Instrument. Pressure was measured with a differential pressure sensor with one input placed at the top of the OWC, beside the orifice, and the other input away from the OWC giving the atmospheric pressure reference.

The 6DOF motion was recorded with a Qualisys motion camera system. Four Oqus cameras are placed above the wave basin and record the linear motion of four spherical markers installed on the OWC. The software generates, using trigonometric equations, the 6DOF motion at the centre of gravity of the OWC floating body based on the relative motion of the four markers and relative position of the centre of gravity and the markers. Placement of the Qualisys markers and pressure sensor location are shown in Figure 12.

ACCEPTED MANUSCRIPT



Figure 12: View of the OWC top section with Qualisys markers, orifice and pressure sensor location.

3.5. List of waves tested

Trials were carried out using a range of regular waves to test the model. Generated waves were calibrated prior to device testing to ensure the accurate propagation of waves. Wave generation for testing the device used the same input settings for the wave calibration stage. A wave height of 20mm was generated with a range of periods from 0.7s to 2.3s. Wave probes are monitored at the same location where the device would be situated during the calibration period. Results for the incident wave heights are presented in Table 3.

Table 3: Incident wave height calibration for each wave period.

T [s]	H [m]
0.69	0.019
0.8	0.021
1	0.021
1.06	0.021
1.14	0.019
1.23	0.020
1.33	0.020
1.59	0.020
1.79	0.020
2	0.020
2.27	0.021

4. Results and discussion

Regular waves are simulated using the comprehensive CFD model described in Section 2.5. Simulations are conducted on multiple clusters of nodes consisting of 24 Xeon cores with 64 GB RAM provided by the Irish Centre for High-End Computing (ICHEC). Monochromatic waves with periods of between 0.8s to 2s are allowed to propagate through the domain with a wave height of 0.02m. Simulations are deemed complete when a quasi-steady state is reached where the heave and pressure drop within the chamber stop changing periodically.

Results for the heave response and pressure drop are plotted in Figure 13 for incident waves with a period of 1.23s. A quasi steady state is observed in both the structural heave and chamber pressure after 10 incident waves. Pressure fluctuation within the chamber shows, as expected, similar non-linear patterns to the results seen in Figures 6 and 7.

Heave results from a range of incident waves were obtained to calculate the heave RAO and subsequently plotted in Figure 14 with experimental results. An excellent agreement is observed between the response of CFD simulations and the experimental data. A peak harmonic is seen with a wave period of 1s in the CFD model, similar to experimental observations.

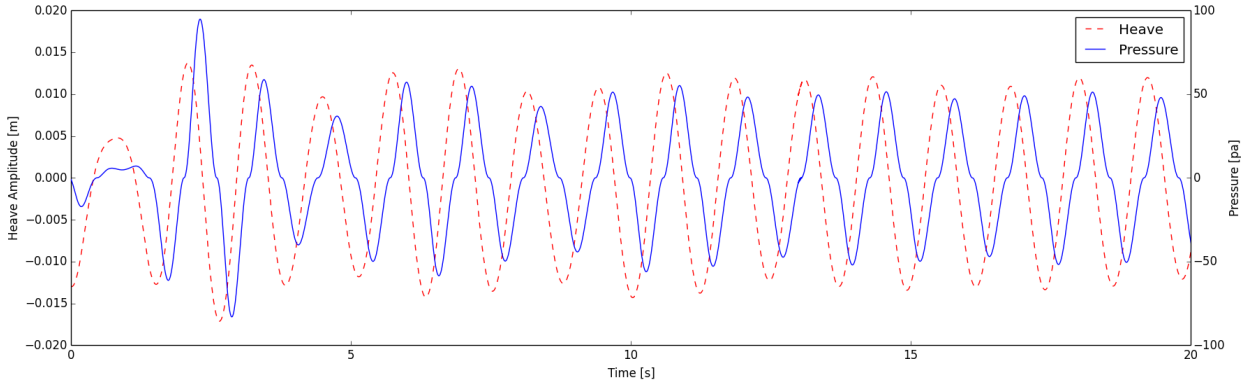


Figure 13: Heave response and pressure plot of a simulation with wave height of 0.02m and period of 1.23s.

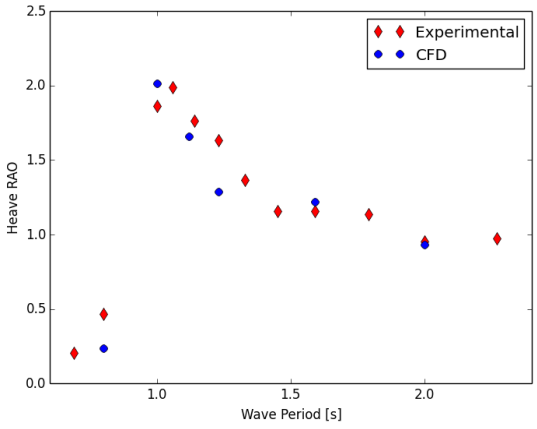


Figure 14: Comparison of CFD and experimental heave RAO plotted with respect to wave period.

Pressure fluctuation within the chamber is recorded and the maximum difference plotted in Figure 15 with respect to wave period. The pressures predicted in the model correspond well with experimental pressure results, although an over estimation is observed at peak resonance. This peak resonance occurs at similar incident wave period as the heave harmonic. The PTO boundary condition previously developed proves to be very promising to replicate and replace the use of an orifice plate in CFD simulations, thereby reducing model complexity.

A smaller secondary peak at a wave period of 1.59s can be seen in Figure 14 which corresponds to the natural frequency of the structure. This secondary peak is observed to be more pronounced in the pressure drop across the PTO, shown by Figure 15. Modification of the structural geometrics allows the user to tune this secondary peak to optimise power output for a specific sea state. Good correlation of the secondary peak is observed between both numerical and experimental data sets. This proves the ability of the numerical model developed here to capture both harmonics of the OWC spar buoy with good accuracy.

5. Conclusion

A CFD model for offshore FSI studies using a commercial package ANSYS Fluent 16.0 is developed in this paper. A 1DOF, heave only, dynamic motion model in 2D is validated against experimental, numerical and analytical work of others using a freely heaving barge. Results from this study demonstrate the accuracy

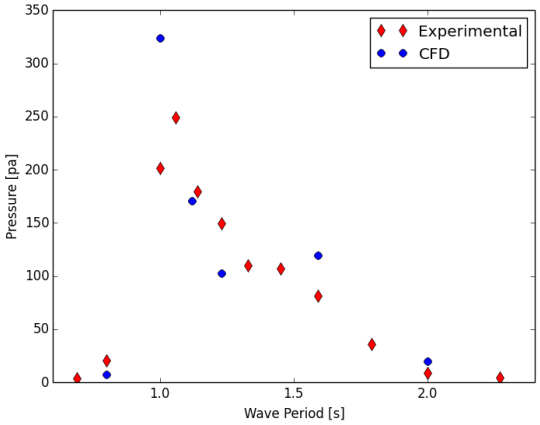


Figure 15: Chamber pressure of the simulation with comparison to experimental work.

of the FSI model set-up. In parallel, a NWT is constructed in 3D to allow for the geometric requirements of a spar buoy OWC to be modelled. This NWT is analysed against theory with various incident waves and shows a high level of accuracy in 3D. A PTO boundary condition is developed to be a robust alternative to modelling an orifice plate. The non-linear PTO boundary is validated with excellent agreement with comparison to experimental results of an orifice plate.

Coupling of the 1DOF, 3D NWT and non-linear PTO boundary condition allowed for a fully dynamic model of a spar buoy OWC to be realised. Numerical simulations show excellent responses to incident waves in both heave and chamber pressure. Replication of the heave and PTO response of the device allows further analysis without the necessity of experimental testing. This permits the evaluation and optimising efficiency of a design with confidence prior to prototype construction. Future model developments will see the inclusion of mooring forces, non-linear incident waves and compressibility interactions for larger scale prototypes.

6. Acknowledgements

The authors would like to acknowledge the financial support provided by the Irish Research Council under the Government of Ireland Postgraduate Scholarship Scheme 2013, grant number GOIPG/2013/1382. The authors also wish to acknowledge the DJEI/DES/SFI/HEA Irish Centre for High-End Computing (ICHEC) for the provision of computational facilities and support. The experimental data used in this work was provided by the MaREI centre in University College Cork and from trials carried out in the LIR-NOTF under the MARINET FP7 funded project with analysis and reporting funded by SFI Grant No. 2/RC/2302.

References

[1] António F.O. Falcão, João C.C. Henriques, and José J. Cândido. Dynamics and optimization of the OWC spar buoy wave energy converter. *Renewable Energy*, 48:369–381, dec 2012.

[2] Kaveh Soleimani, Mohammad Javad Ketabdari, and Farzan Khorasani. Feasibility study on tidal and wave energy conversion in Iranian seas. *Sustainable Energy Technologies and Assessments*, 11:77–86, 2015.

[3] R P F Gomes, J C C Henriques, L M C Gato, and António F.O. Falcão. Testing of a small-scale floating OWC model in a wave flume. In *International Conference on Ocean Energy*, pages 1–7, 2012.

[4] T. W. Thorpe. An Overview of Wave Energy Technologies : Status , Performance and Costs. In *Wave Power: Moving Towards Commercial Viability*, number November, pages 1–16. IMechE, 1999.

[5] António F.O. Falcão and João C.C. Henriques. Oscillating-water-column wave energy converters and air turbines: A review. *Renewable Energy*, 85:1391–1424, 2016.

[6] Jiyuan Tu, Guan Heng Yeoh, and Chaoqun Liu. *Computational Fluid Dynamics: A Practical Approach*. Elsevier, second edition, 2008.

ACCEPTED MANUSCRIPT

[7] B Bouali and S Larbi. Contribution to the Geometry Optimization of an Oscillating Water Column Wave Energy Converter. *Energy Procedia*, 36:565–573, 2013.

[8] Arun Kamath, Hans Bihs, and Øivind A Arntsen. Numerical modeling of power take-off damping in an Oscillating Water Column device. *INTERNATIONAL JOURNAL OF MARINE ENERGY*, 10:1–16, 2015.

[9] E Didier, J M Paixão Conde, and P R F Teixeira. NUMERICAL SIMULATION OF AN OSCILLATING WATER COLUMN WAVE ENERGY CONVERTER WITH AND WITHOUT DAMPING MARINE 2011. In *International Conference on Computational Methods in Marine Engineering*, pages 1–12, 2011.

[10] Yongyao Luo, Zhengwei Wang, Guangjie Peng, Yexiang Xiao, Liming Zhai, Xin Liu, and Qi Zhang. Numerical simulation of a heave-only floating OWC (oscillating water column) device. *Energy*, pages 1–8, sep 2014.

[11] Ken O Connell and Andrew Cashman. Development of a numerical wave tank with reduced discretization error. In *International Conference on Electrical, Electronics, and Optimisation Techniques (ICEEOT)*, in press.

[12] ANSYS Fluent 16.0 Theory Guide.

[13] Mihoko Nojiri and Hitoshi Murayama. A study on the drift force on two dimensional floating body in regular waves. In *Trans. West-Japan Soc. Nav. Arch*, volume 51, pages 131–152, 1975.

[14] Weoncheol Koo and Moo-Hyun Kim. Freely floating-body simulation by a 2D fully nonlinear numerical wave tank. *Ocean Engineering*, 31(16):2011–2046, nov 2004.

[15] Yongyao Luo, Jean-Roch Roch Nader, Paul Cooper, and Song-Ping Ping Zhu. Nonlinear 2D analysis of the efficiency of fixed Oscillating Water Column wave energy converters. *Renewable Energy*, 64:255–265, apr 2014.

[16] Katsuji Tanizawa and Makiko Minami. On the Accuracy of NWT for Radiation and Diffraction Problem. In *6th Symposium for Nonlinear and Free-Surface Flow*, pages 1–4, 1998.

[17] Florent Thiebaut, J Griffiths, A Pellat, D O Sullivan, and R Alcorn. Servomotor controlled piston rig for the simulation of an Oscillating Water Column air chamber. *Proceedings of the 3rd International Conference on Ocean Energy*, pages 1–6, 2010.

ACCEPTED MANUSCRIPT

ACCEPTED MANUSCRIPT

- Discretization analysis of incident waves in a 3D NWT using CFD software
- Development and validation of a non-linear orifice plate boundary for PTO simulation
- Detailed description on experimental work completed on a Spar buoy OWC
- Construction of a 1DOF, heave only, Spar buoy OWC with non-linear PTO simulator
- Analysis and validation of developed comprehensive dynamic OWC model

ACCEPTED MANUSCRIPT